Composite membranes with hydrophilic nanopores derived from the self-assembly of block copolymer supramolecular complexes

Composite membranes with hydrophilic nanopores derived from the self-assembly of block copolymer supramolecular complexes

L. Iannarelli[1], R. Nisticò[1], P. Avetta[1], M. Lazzari[2], G. Magnacca[1,3], P. Calza[1,3], D. Fabbri[1], D. Scalarone*[1,3]

[1] *Department of Chemistry, University of Torino, Via P. Giuria 7, 10125 Torino, Italy*
[2] *Centre for Research in Biological Chemistry and Molecular Materials (CIQUS), University of Santiago de Compostela, 15782 Santiago de Compostela, Spain*
[3] *NIS Centre, University of Torino, Via P. Giuria 7, 10125 Torino, Italy*

*Corresponding author:
Dominique Scalarone
Department of Chemistry
Via P. Giuria 7, 10125 Torino, Italy
Phone: +39 0116707546 - Fax: +39 0116707855
e-mail: dominique.scalarone@unito.it

Abstract

Selective composite membranes with high and controlled porosity have been fabricated using patterned silicon microsieves as support and nanoporous polystyrene-*block*-poly(ethylene oxide) (PS-*b*-PEO) membranes as selective layer. The desired morphology of the block copolymer layer is obtained by a supramolecular approach based on the hydrogen bonding of the PEO block with resorcinol. The formation of PS-*b*-PEO/resorcinol complexes allows to easily control the self-assembly of the block copolymer and to obtain normally oriented PEO/resorcinol nanocylinders by spin coating PS-*b*-PEO/resorcinol solutions. In a further step resorcinol works as a porogen and by its selective dissolution densely packed, normally oriented nanochannels coated by PEO chains have been obtained. These hydrophilic nanochannels have a diameter of approximately 20 nm and cross the membranes from top to bottom. The nanoporous polymer layer is crack-free and well adheres to the support microsieve. The composite membrane is permeable to methylene blue while blocks larger molecules, such as bovine serum albumin.

Keywords

Composite membranes, supramolecular complexes, nanopores, block copolymers, selectivity

1. Introduction

The capability of block copolymers to spontaneously arrange into well-defined ordered structures with nanoscopic size has proven to be particularly advantageous for templating nanoporous materials ranging from oxidic monoliths to inorganic and polymeric thin films.[1-6] Self-assembling of block copolymer templates has been also proposed as an alternative strategy to phase inversion,[7-8] track-etched[9-10] and lithographic techniques[11] for the fabrication of nanoporous polymer membranes with high and controlled porosity.

The simplest strategy to obtain membranes from self-assembled block copolymers envisages the removal of the minority block (i.e. the lower molecular weight block of the block copolymer), while the majority one forms a continuous matrix. Block copolymer assemblies resulting in the cylindrical morphology and with cylinder orientation normal to the film surface are the most interesting ones as they allow the fabrication of membranes with highly ordered channels spanning the whole membrane thickness.[12] The main advantages of block copolymer-templated membranes over other types of polymer membranes are their narrow pore size distribution, high void fraction and smooth surfaces, resulting in superior selectivity, high fluxes and fouling resistance.[13,14] Pore size can be easily varied to optimize size selectivity, and additional separation mechanisms can be introduced by tuning the membrane surface properties through functionalization of the pore walls.[15-17]

Most preparative protocols for nanoporous membranes derived from block copolymers consist in: 1) deposition of block copolymer solutions on proper supports, 2) annealing of the resulting thin films in order to optimize phase segregation and orientation of polymer domains, 3) pore generation. Through the deposition and annealing steps nanostructured thin films are obtained which consist of ordered nanosized domains (i.e. nanocylinders) embedded in a continuous matrix

of the majority block.[18] In the third step block copolymer films are transformed in nanoporous membranes by elimination of a minor component through methods that do not compromise the integrity of the matrix material. This may be accomplished by selective degradation of the minority block or by selective dissolution of additional components, such as small organic molecules or homopolymers [19-21] confined within the minority block domains.

Recently block copolymer-derived membranes have been proposed as highly selective layers in composite membranes.[22,23] Highly selective separations and high flux have been obtained by membranes with an asymmetric film geometry consisting in a thin nanoporous layer, prepared from a block copolymer, and a support membrane. Both polymeric[24,25] and silicon macroporous supports[23] have been proposed for the fabrication of composite membranes.

In this contribution, we describe the fabrication procedure of nanoporous membranes with uniform pore size and high pore density obtained by spin-coating polystyrene-*block*-poly(ethylene oxide) (PS-*b*-PEO) solutions on commercial silicon microsieves. The desired morphology and orientation of the block copolymer domains is achieved by a supramolecular approach based on the complexation by hydrogen-bonding of the PEO block with hydroxyl groups of resorcinol (RES) molecules. The major advantage of the supramolecular approach is that the low molecular weight molecule (i.e. resorcinol) can be easily removed by solvent rinsing, leaving a nanoporous material with the same morphology as the parent material. In a previous paper we demonstrated that the changed interfacial interactions and the reduction in the crystalline PEO phase due to the presence of RES are able to force the complexated PS-*b*-PEO copolymers to self-segregate giving perpendicular oriented PEO/RES cylinders.[26]

Starting from that finding ordered nanostructured films with normally oriented PEO/RES cylindrical domains were prepared. These films were subjected to a mild photo-degradation by UV treatment, both to improve their mechanical resistance by crosslinking the PS matrix, and to increase their hydrophylicity by introducing polar groups on the PEO chains. Pores were then generated by selective dissolution of RES embedded in the cylindrical PEO domains. PEO-coated

nanochannels crossing the membrane thickness were thus obtained. Permeability and selectivity of the composite membrane were assessed by monitoring the diffusion of methylene blue (MW=320 g mol^{-1}) and bovine serum albumin (MW=66 Kg mol^{-1}).

2. Experimental

2.1. Materials

PS_{308}-*b*-PEO_{250} (M_n=32000-*b*-11000) was purchased from Polymer Source Inc. (Dorval, Canada) and used without further purification.

Resorcinol (RES ≥99%) was obtained by Carlo Erba. Benzene, 2-propanol, diethyl ether, acetic acid (HAc), methylene blue (MB), bovine serum albumin (BSA), sodium dihydrogenphosphate and sodium hydroxide were purchased from Sigma Aldrich.

2.2. Preparation of nanoporous membranes

Copolymer benzene solutions (2 wt%) were stirred for half an hour to ensure complete dissolution of the copolymer. Then resorcinol was added in order to obtain mixtures with a molar ratio RES:EO of 1:2, 1:4 and 1:8. Prior to deposition solutions were filtered through 0.45 μm PTFE membrane syringe filters. A few drops of each solution were spin coated onto proper supports at 1000 rpm for 20 sec, using a 8" Desk-top Precision Spin Coating System, model P-6708D vs. 2.0. Films were dried in a hood at ambient temperature for at least 12 h and then were UV-irradiated for 8 h under a fluorescent lamp (Philips TUV T8) emitting UV-C rays at 15 W. Finally, nanopores were generated by immersing the films into solvents able to selectively dissolve RES. Following this procedure nanoporous polymer membranes were prepared on dense supports (mica, glass and silicon) and on commercial silicon microsives by Aquamarijn Micro Filtration BV (Zutphen, Netherlands), having on top a Si_3N_4 membrane with surface area of 5 x 5 mm, thickness of 0.6 mm and pores of 5 μm in diameter arranged in hexagonal setting.

2.3. Characterization

Surface morphology of both nanostructured PS-b-PEO/RES films and of nanoporous membranes obtained after resorcinol removal was studied by Atomic Force Microscopy operating in Non-Contact mode (AFM-NC). Analyses were performed in air at room temperature with a Park Systems Instrument, model XE-100. A silicon microcantilever with the reflective side coated with aluminum (force constant 20 N/m and resonance frequency of 265 kHz) and conical silicon tips (radius of curvature less than 10 nm, tip height 15-20 µm, full tip cone angle less than 30°) were used. Scan rates were set between 0.5 and 1 Hz.

Field Emission Scanning Electron Microscopy (FESEM) images were obtained with a Zeiss Ultra Plus field emission SEM at 1.5-3.0 kV (range of acceleration voltage: 0.02 kW – 30 kW) equipped with an Inlens detector and a SE Everhart - Thornley Secondary Electron Detector. For FESEM analyses nanoporous membranes were prepared on silicon wafers. Areas close to fracture lines were observed in order to get information on the shape, size, distribution and alignment of the pores within the membrane thickness.

Integrity and large-scale homogeneity of the membranes prepared both on dense substrates (i.e. mica and silicon discs) and on silicon microsieves were assessed by a Leica DM2005 optical microscope equipped with a digital camera for image acquisition and by scanning electron microscopy (SEM). SEM analyses were carried out using a ZEISS EVO 50 XVP with LaB_6 source, equipped with detectors for secondary electrons collection and EDS probe for elemental analyses.

Fourier Transform Infrared Spectroscopy (FTIR) spectra were collected with a Thermo-Nicolet FTIR Nexus instrument with a DTGS detector operating in transmission mode and in attenuated total reflectance (ATR) mode. For infrared analysis in transmission mode samples were prepared by solvent casting on silicon wafers and spectra were collected in the spectral range of 4000-400 cm^{-1}, with a resolution of 4 cm^{-1} and 32 scans. ATR spectra were collected with a Thermo Nicolet Smart Endurance device.

Thermal analysis were carried out with a Q200 (TA Instruments) Differential Scanning Calorimeter equipped with a refrigerated cooling system in the temperature range from -80 to 150 °C, with a scanning rate of 10 °C/min and under nitrogen atmosphere.

2.3. Transport tests

Transport tests were carried out by using a homemade side-by-side diffusion cell consisting of two half-cells in Pyrex physically separated by the porous membrane, fixed by two silicone seals covered with Teflon and held together with a metal clamp. The sealing of the system was evaluated with diffusion tests performed in the presence of square metal in place of the membrane. TOC analysis excluded the release of organic impurities from every part of the device. The TOC analysis were carried out with a Shimadzu TOC-VCSH Total Organic Carbon Analyzer, equipped with an ASI-V autosampler and fed with zero-grade air (Sapio, Italy).

The solution of target molecule, MB (5.0×10^{-4} mol L^{-1}, water solution) and BSA (1.0 %, phosphate buffer solution pH 7.0), was put in the donor cell and the passage through the membrane was evaluated by means of UV-Visible spectrophotometric analysis (CARY 100 Scan-Varian spectrophotometer) performed on the solution in the receptor cell (filled with water for MB and with phosphate buffer solution pH 7.0 for BSA). The diffusion tests were carried out with continuous stirring in both cells. The spectrophotometric determination of target molecules was done at 664 nm for the dye and 280 nm for the albumin, and quantification was performed with external calibration curves ($r^2 \geq 0.9996$ for MB and $r^2 \geq 0.9991$ for BSA). Reported data are averages of three replicas.

3. Results and Discussion

Most applications of block copolymer-based coatings in nanotechnology require the achievement of a cylindrical morphology with cylinders oriented normally to the material surface. A straightforward method to prepare nanostructured films with this morphology is based on the

addition to block copolymer solutions of small molecules that preferentially interacts with one of the blocks. Salt complexation, as well as hydrogen bonding between labile hydrogen atoms of organic molecules and one of the copolymer blocks, can dramatically affect the orientation of cylindrical nanodomains producing normally orientated cylinder arrays with enhanced lateral order.[19, 27] Hydrogen bonding between RES and EO units was used to direct the orientation of PEO cylinders in PS-*b*-PEO copolymers and to produce nanostructured coatings with normally oriented PEO/RES cylinders in a PS matrix.[26]

We decided to apply the same supramolecular strategy to prepare PS-*b*-PEO nanoporous membranes using RES both to obtain the desired morphology and as a porogen, as it can be easily removed from PS-*b*-PEO films by dissolution in selective solvents.

The first stage of this research was addressed to investigate the effect of different amounts of RES on the physico-chemical properties of nanostructured PS-*b*-PEO/RES films. PS-*b*-PEO/RES films with a RES:EO molar ratio of 1:2, 1:4 and 1:8 were prepared on dense supports (i.e. silicon wafers, glass and mica) and characterized. In Figure 1 the infrared spectra of RES and of the complexated block copolymers are reported. Formation of hydrogen bonding between EO units and RES molecules is proved by the shift observed for the OH stretching band in spectra 1b-1d: if RES interacts with PEO, the extended H-bonding system typical of pure RES is broken and the stretching signal shifts to higher frequency. In particular, the presence of a maximum at 3315 cm^{-1} is specific for the hydrogen bonding interaction between RES and oxygen atoms of the PEO block.[28] Absorptions between 1000 and 1300 cm^{-1} are mainly due to C-O-C and C-O-H vibrations of EO and RES. In spectrum b) of Figure 1, which refers to the polymer sample containing the highest amount of RES, these absorptions are complex and they result from the superimposition of different, sharper contributions, as it is for a crystalline material, while spectra c) and d) show a broader and smooth absorption that indicates a relevant reduction of the crystalline component.

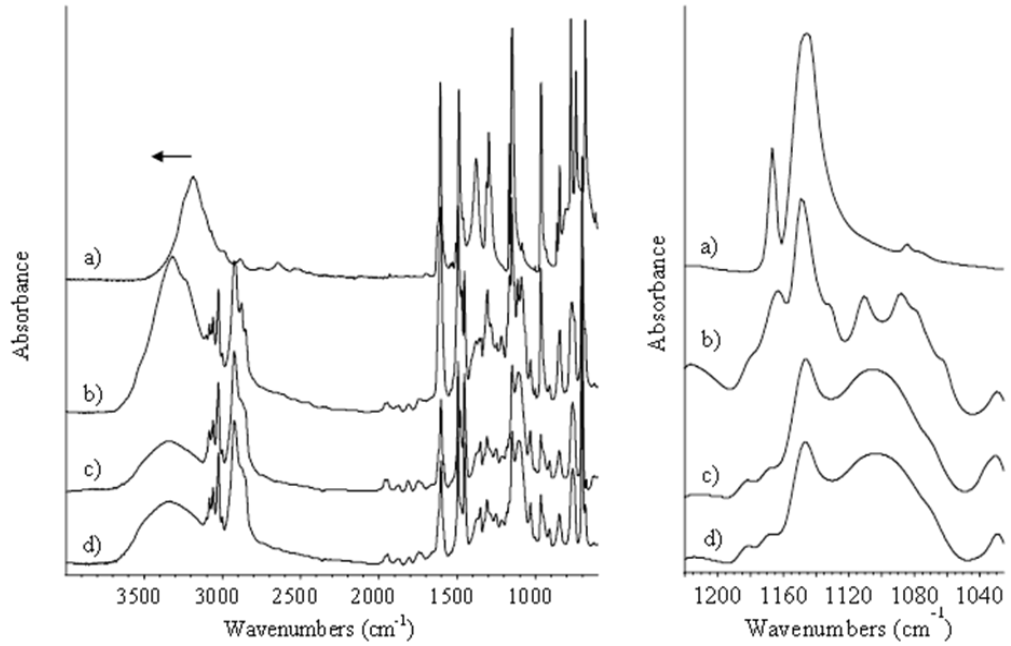

Figure 1. FTIR spectra of RES (a), PS-*b*-PEO/RES, RES:EO 1:2 (b), PS-*b*-PEO/RES, RES:EO 1:4 (c), PS-*b*-PEO/RES, RES:EO 1:8 (d).

The presence of strong interactions existing between RES and PEO blocks and the different crystalline degree shown by the analyzed samples were confirmed by calorimetric analyses. Compared to the melting signal of the pure copolymer (Figure 2, curve a), in PS-*b*-PEO/RES films melting is always shifted at higher temperature and this is consistent with the presence of a

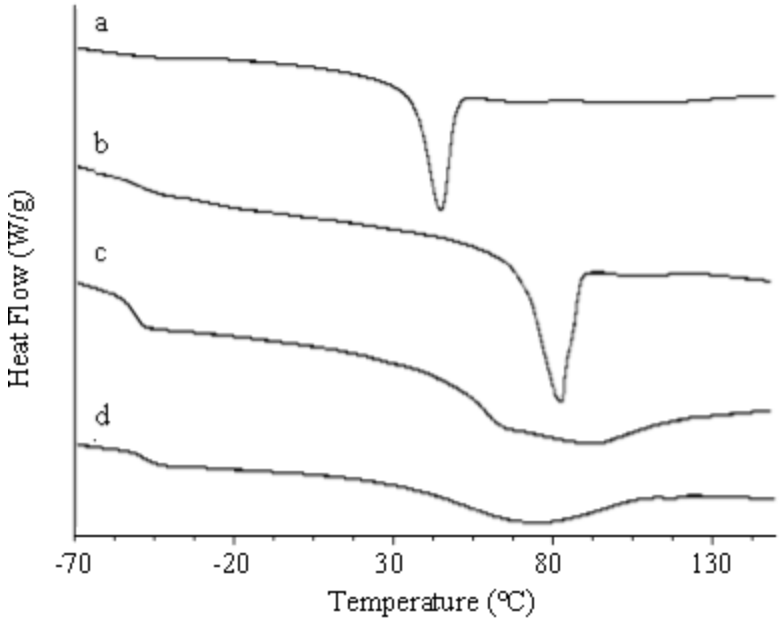

Figure 2. DSC curves of PS-*b*-PEO (a), PS-*b*-PEO/RES, RES:EO 1:2 (b), PS-*b*-PEO/RES, RES:EO 1:4 (c), PS-*b*-PEO/RES, RES:EO 1:8 (d).

PEO/RES crystalline complex.[29] In particular, the intense and relatively sharp melting peak of the film with EO and RES in stoichiometric ratio (curve b) can be assigned to the α form of the crystalline 1:2 molar ratio RES/PEO complex, which is a rather stable crystalline form. With respect to this, the melting signals of the films with a RES:EO molar ratio of 1:4 and 1:8 (curves c and d respectively) are broader and less intense demonstrating that in these films the morphology of the crystalline phase is less homogeneous and the degree of crystallinity is considerably reduced. This reduction in the crystalline phase is also confirmed by the heat flow changes due to the glass transition: in curves c and d of Figure 2 the glass transition of the PEO/RES phase can be easily detected at approximately -50°C, while it is hardly detectable in the DSC curves of the other two samples whose PEO phase is mainly crystalline. Overall these results confirm that when the RES:EO molar ratio is 1:4 or lower the amount of crystalline phase is negligible and the PS-*b*-PEO/RES films are basically amorphous. This is an important aspect of the overall membrane fabrication procedure as amourphous polymers are better film-forming materials than semi-crystalline polymers and they are expected to give films (and membranes) of better quality. In fact, optical microscopy analyses of these films demonstrate that their surface is continuous and homogenous, and AFM images show a regular array of densely packed PEO/RES cylinders with perpendicular orientation (Figure 3a). Thus, PS-*b*-PEO/RES films with a molar ratio RES:EO 1:4 were selected as ideal candidates for the fabrication of nanoporous membranes.

Films were irradiated by UV light for 8 h to improve their mechanical and solvent resistance by crosslinking the PS matrix.[30] Infrared spectra of irradiated samples (here not reported for sake of brevity) show the appearance of a band at 1730 cm^{-1}, which is assigned to the stretching of carbonyl groups formed by photooxidative degradation of the PEO block.[31] The carbonyl absorption is very low after 8 h of UV treatment and it increases considerably only for longer irradiation times, which indicates that the PEO chains are not very affected by the UV treatment except for the formation of polar groups that make the irradiated films more hydrophilic than the non-irradiated ones. No morphological changes were observed within 8 h of UV irradiation.

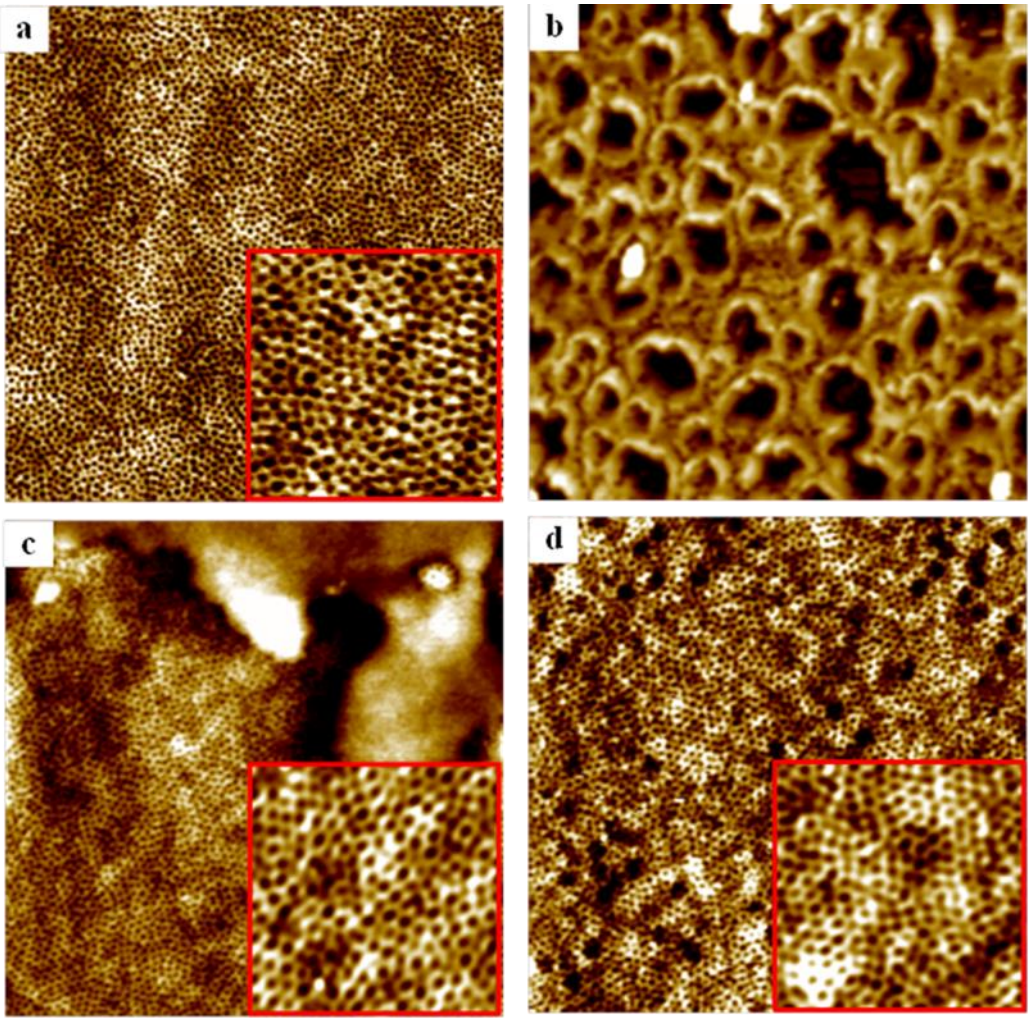

Figure 3. 2×2 μm AFM images of nanostructured films PS-*b*-PEO/RES, RES:EO 1:4 before (a) and after solvent treatments with ethyl ether for 1 min (b), HAc /H_2O 75/25 for 10 min (c) and 2-propanol for 30 min (d). Boxed images are 500×500 nm.

To selectively remove RES from the nanostructured films five solvent systems were tested: diethyl ether, acetic acid, 2-propanol, water and acetic acid/water 75/25 (v/v) solution. The removal of resorcinol from the films was followed by infrared spectroscopy by monitoring the decreasing of characteristic absorption bands of RES versus immersion time. The film morphology was observed by AFM before and after solvent treatments. Although water is a good solvent for RES, it was unable to remove it from the nanostructured films even after several hours of immersion. After only one minute of immersion in acetic acid the nanostructured films detached from the solid support. Diethyl ether seemed very effective in removing RES, but the film morphology was severely damaged by the treatment loosing completely its characteristic nanostructure (Figure 3b). The acetic acid/water solution was able to completely remove resorcinol in 10-20 minutes of immersion,

without affecting the nanostructure, but partial detachment of the film from supports was observed (Figure 3c). 2-Propanol selectively dissolved RES in 30-60 minutes of immersion depending on the film thickness, and without affecting the film nanostructure (Figure 3d).

Complete removal of RES was also confirmed by DSC: the curve of the PS-b-PEO/RES films after 30 minutes of treatment in 2-propanol does not show any thermal transition indicating the presence of RES or RES/EO complexes, and melting occurs in the same temperature range expected for the PEO component of the pure block copolymer.

The removal of RES from the nanostructured films generates a porosity in the PEO cylinders and the collapse of PEO chains onto the pore walls. As a result a dense array of nanosized channels spanning the film thickness is obtained. FESEM micrographs in Figure 4 show a detail of the membrane close to a fracture line that has been produced in order to offer at the same time a view of the membrane morphology at the surface and along the thickness. Cylindrical, normally oriented pores are regularly packed and extend over the entire membrane area. The fracture exposes the inner part of the membrane and demonstrates that channels are straight and cross the membranes from top to bottom. Pore size, as determined from FESEM and AFM images of membranes dried in air, is approximately 20 nm. However, it must be considered that once in water PEO chains are hydrated and reasonably they occupy a larger volume.

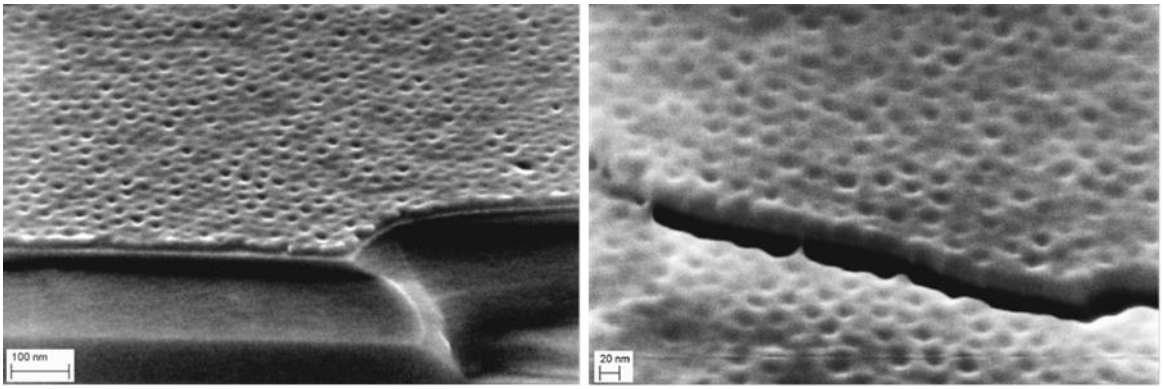

Figure 4. FESEM micrographs of nanoporous PS-*b*-PEO membranes supported on a silicon wafer.

The next step of the research was aimed at the fabrication of a composite membrane suitable to be integrated in miniaturized devices for filtration and controlled transport of molecules in solution. Block copolymer-templated membranes were fabricated on silicon microsieves provided of a Si_3N_4 surface membrane with pores arranged in a hexagonal setting and having a diameter of 5 μm. A couple of drops of block copolymer solution were poured on the microsieve surface. As wetting of the block copolymer solution is little, the drop does not infiltrate the microsieve pores, but stands on the surface as it would be for flat substrates. Thus, spin coating can be applied to spread the polymer solution and deposit a uniform film having a thickness of approximately 50-60 nm, as measured by AFM. After UV treatment and immersion in 2-propanol for 30 minutes, a polymer nanoporous layer was obtained. This polymer membrane is continuous and crack-free over a large area and well adheres to the Si_3N_4 surface. It is visible as an opaque layer in the left side of the SEM micrograph of Figure 5, while the right side, that shows the neat surface of the microsieve, is characterized by a higher contrast between the black pores and the bright Si_3N_4 membrane. The

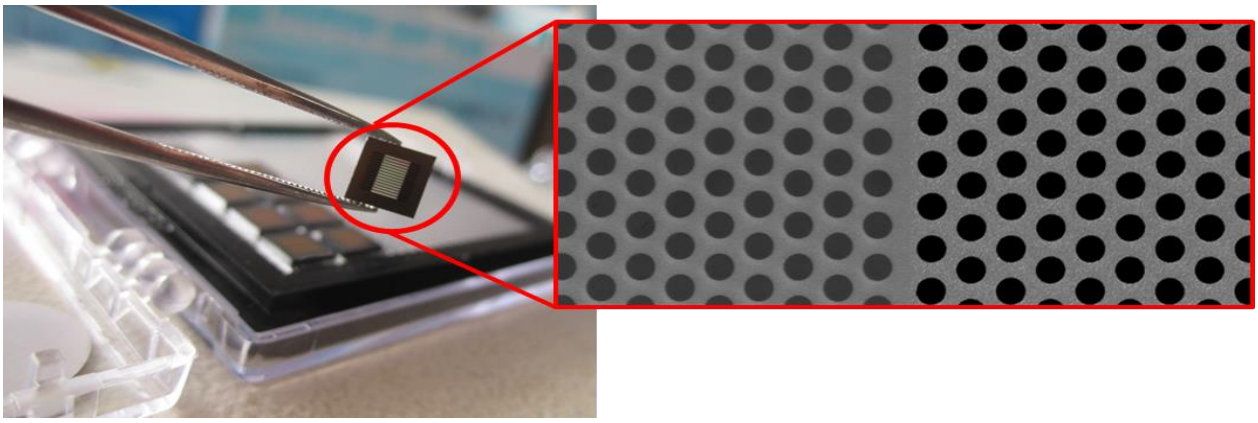

Figure 5. Silicon microsieves (5×5×0.6 mm) used to support the nanoporous membranes. SEM micrographs show the Si_3N_4 macroporous membrane on top of the microsieve. Pores have diameter of 5 μm. The SEM micrograph on the right refers to a blank microsieve and the image on the left refers to a microsieve with a nanoporous membrane on top.

good coverage of the large pores of the microsieve by the nanoporous polymer membrane is definitely confirmed by AFM analyses reported in Figure 6. The nanoporous membrane perfectly adheres to the microsieve and covers the 5 μm pores from side to side without fractures (Figure 6a-b). On these areas the nanoporous membrane is slightly bended, but the profile line in Figure 6c and the corrected AFM image obtained by flattening the curvature of the profile lines clearly show that the nanoporous polymer is a continuous thin layer on top of the microsieve. This also proves that the nanoporous membrane, although very thin, has good mechanical properties and it is able to maintain its mechanical integrity during the entire fabrication procedure, including the solvent treatment required to generate pores. Figure 6d shows that the desired alignment of the nanochannels is maintained throughout the whole membrane, even where the nanoporous membrane is hanging over the macropores of the microsieve support.

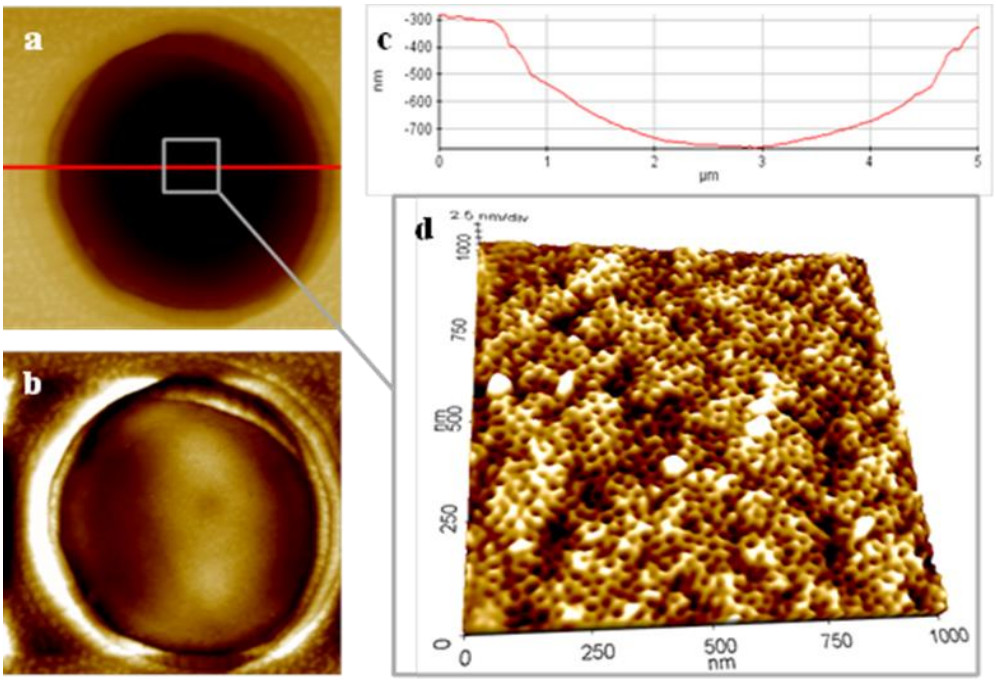

Figure 6. AFM images of a composite nanoporous membrane: detail of the microsieve with the nanoporous polymer membrane on top (a); corrected AFM image showing the coverage of the macropore by the polymer membrane (b); AFM profile corresponding to the horizontal line in Figure 6a (c); 3D AFM image showing the morphology of the nanoporous layer (d).

Transport studies were carried out monitoring by UV-Vis spectroscopy the diffusion through the composite membrane of two molecules with different size, i.e. MB and BSA. The hydrodynamic radius of MB is 0.5 nm [32], while that of BSA is approximately 3.5 nm,[33] thus according to these values both molecules should cross the membrane. In Figure 7 the percentage ratio between the concentration at different times and the concentration at the equilibrium (half of the starting concentration) is reported versus time. Diffusion curves demonstrate that dye molecules cross the membrane while albumin is blocked. In addition, permeability was evaluated by calculating the diffusion rate at t_0, i.e. tangent of the diffusion curve at t_0, and results demonstrate that BSA permeability is approximately 500-fold lower than MB.

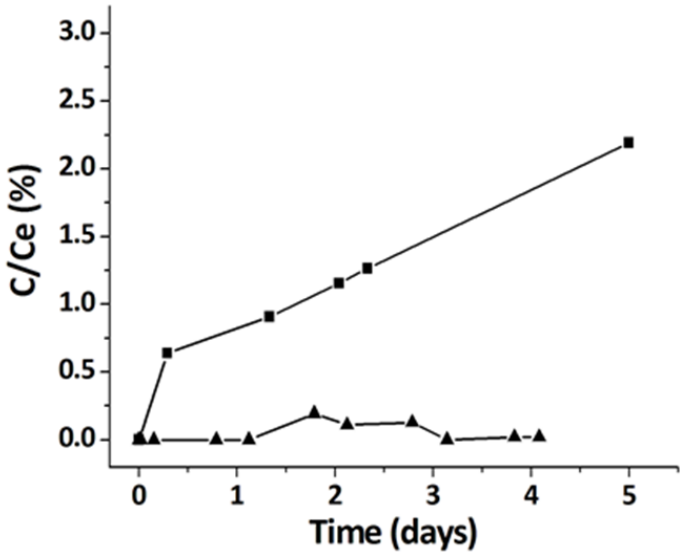

Figure 7. MB (squares) and BSA (triangles) diffusion through the composite membrane.

This can be explained taking into account that the pore size of 20 nm was determined on dry membranes where PEO blocks are collapsed on the pore walls, but once in water the hydrated PEO chains occupy a larger volume, thus reducing the effective pore diameter and blocking BSA. By sure BSA, having an higher molecular mass, has a lower diffusion coefficient (D) in free solution than MB, but the difference in diffusivity is not enough to justify in itself the permeability results of Figure 7. Diffusion coefficients of MB and BSA in free solution were calculated by using the Stokes-Einstein equation:

$$D = \frac{k_B T}{6\pi\eta R_h}$$

where k_B is the Boltzmann constant, T the absolute temperature and η the viscosity of the solution. For dilute solutions used in the experiments, viscosity of both MB and BSA solutions may be assumed to be that of water at that temperature. This way the diffusion coefficient of MB in free solution results to be only 7-fold higher than the diffusion coefficient of BSA. This value is negligible if compared to the 500-fold permeability difference resulting from data of Figure 7, thus confirming the capability of the nanoporous composite membrane to improve the selectivity of the separation process.

4. Conclusions

The fabrication of nanoporous membranes with well-defined uniform pore size and high pore density opens new perspectives in separation processes, in dosing of chemicals and in the design and fabrication of miniaturized devices for drug release. Here we have described a simple procedure for the fabrication of composite membranes with a nanoporous top layer that can be easily integrated in microfluidic devices. The nanoporous layer is prepared by a supramolecular approach which allows to finely control the pore shape, size and orientation.

Acknowledgements

Compagnia di San Paolo and University of Torino are gratefully acknowledged for funding Project ORTO114XNH through "Bando per il finanziamento di progetti di ricerca di Ateneo - anno 2011". M. L. also thanks the financial support by the Spanish Ministerio de Educación, Cultura y Deporte (MAT2012-36754-C02-01) and the Xunta de Galicia (GRC2013-044 FEDER funds)

References

[1] G. J. A. A. Soler-Illia, E. L. Crepaldi, D. Grosso, C. Sanchez, *Curr. Opin. Colloid Interface Sci.* **2003**, *8*, 109.

[2] K. Yu, B. Smarsly, C. J. Brinker, *Adv. Funct. Mater.* **2003**, *13*, 47.

[3] R. Nisticò, D. Scalarone, G. Magnacca, *Microporous and Mesoporous Mater.* **2014**, *190*, 208.

[4] T. Liu, C. Burger, B. Chu, *Prog. Polym. Sci.* **2003**, *28*, 5.

[5] R. A. Segalman, *Mater. Sci. Eng. R.* **2005**, *48*, 191.

[6] A. Laforgue, C. G. Bazuin, R. E. Prud'homme, *Macromolecules* **2006**, *39*, 6473.

[7] M. Ulbricht, *Polymer* **2006**, *47*, 2217.

[8] S. P. Nunes, *Trends Polymer Sci.* **1997**, *5*, 187.

[9] R. L. Fleischer, P. B. Price, and R. M. Walker, *Nuclear Tracks in Solids. Principles and Applications*, University of California Press, Berkeley **1975**.

[10] P. Apel, *Radiat. Meas.* **2001**, *34*, 559.

[11] F. Martin, R. Walczak, A. Boiarski, M. Cohen, T. West, C. Cosentino, M. Ferrari, *J. Control. Release* **2005**, *102*, 123.

[12] E. A. Jackson, M. A. Hillmyer, *ACS Nano* **2010**, *4*, 2548.

[13] W. A. Phillip, M. Amendt, B. O'Neill, L. Chen, M. A. Hillmyer, E. L. Cussler, *ACS Appl. Mater. Interfaces* **2010**, 2, 472.

[14] X. Zhu, M. Elimelech, *Environ. Sci. Technol.* **1997**, 31, 3654.

[15] S. Ndoni, L. Li, L. Schulte, P. P. Szewczykowski, T. W. Hansen, F. X. Guo, R. H. Berg, M. E. Vigild, *Macromolecules* **2009**, *42*, 3877.

[16] H. Mao, P. L. Arrechea, T. S. Bailey, B. J. S. Johnsonw, M. A. Hillmyer, *Faraday Discuss.* **2005**, *128*, 149

[17] J. Rzayev, M. A. Hillmyer, *J. Am. Chem. Soc.* **2005**, *127*, 13373.

[18] I. W. Hamley, *The Physics of Block Copolymers*, Oxford University Press, Oxford, 1998.

[19] A. Sidorenko, I. Tokarev, S. Minko, M. Stamm, *J. Am. Chem. Soc.* **2003**, *125*, 12211

[20] A. Laforgue, C. G. Bazuin, R. E. Prud'homme, *Macromolecules* **2006**, *39*, 6473.

[21] U. Jeong, H.-C. Kim, R. L. Rodriguez, I. Y.Tsai, C. M. Stafford, J. K. Kim, C. J. Hawker, T. P. Russell, *Adv. Mater.* **2002**, *14*, 274.

[22] S. Y. Yang, J. A. Yang, E. S. Kim, G. Jeon, E. J. Oh, K. Y. Choi, S. K. Hahn, J. K. Kim, *ACS Nano* **2010**, *4*, 3817.

[23] E. E. Nuxoll, M. A. Hillmyer, R. Wang, C. Leighton, R. A. Siegel, *ACS Appl. Mater. Interfaces* **2009**, *1*, 888.

[24] W. A. Phillip, B. O'Neill, M. Rodwogin, M. A. Hillmayer, E. L. Cussler, *ACS Appl. Mater. Interfaces* **2010**, *2*, 847.

[25] S. Y. Yang, I. Ryu, H. Y. Kim, J. K. Kim, S. K. Jang, T. P. Russell, *Adv. Mater.* **2006**, *18*, 709.

[26] D. Scalarone, J. Tata, M. Lazzari, O. Chiantore, *Eur. Polym. J.* **2009**, *45*, 2520.

[27] S. H. Kim, M.J. Misner, L. Yang, O. Gang, B. M. Ocko, T. P. Russell, *Macromolecules* **2006**, *39*, 8473.

[28] J. Spěváček, L. Paternostre, P. Damman, A. C. Draye, M. Dosière, *Macromolecules* **1998**, *31*, 3612.

[29] H. Schmalz, V. Abetz, A.J. Müller, *Macromol. Symp.* **2002**, *183*, 179.

[30] B. Ranby J.F. Rabek, *Photodegradation, Photo-Oxidation and Photostabilization of Polymers*, Wiley, New York **1975**.

[31] P. de Saint Claire, *Macromolecules* **2009**, *42*, 3469.

[32] M. Majumder, P. Sheath, J. I. Mardel, T. G. Harvey, A. W. Thornton, A. Gonzago, D. F. Kennedy, I. Madsen, J. W. Taylor, D. R. Turner, M. R. Hill, *Chem. Mater.* **2012**, *24*, 4647.

[33] I. Axelsson, *J Chromatogr. A* , **1978**, *152*, 21.

Figure captions

Figure 1. FTIR spectra of RES (a), PS-*b*-PEO/RES, RES:EO 1:2 (b), PS-*b*-PEO/RES, RES:EO 1:4 (c), PS-*b*-PEO/RES, RES:EO 1:8 (d).

Figure 2. DSC curves of PS-*b*-PEO (a), PS-*b*-PEO/RES, RES:EO 1:2 (b), PS-*b*-PEO/RES, RES:EO 1:4 (c), PS-*b*-PEO/RES, RES:EO 1:8 (d).

Figure 3. 2×2 μm AFM images of nanostructured films PS-*b*-PEO/RES, RES:EO 1:4 before (a) and after solvent treatments with ethyl ether for 1 min (b), HAc /H_2O 75/25 for 10 min (c) and 2-propanol for 30 min (d). Boxed images are 500×500 nm.

Figure 4. FESEM micrographs of nanoporous PS-*b*-PEO membranes supported on a silicon wafer.

Figure 5. Silicon microsieves (5×5×0.6 mm) used to support the nanoporous membranes. SEM micrographs show the Si_3N_4 macroporous membrane on top of the microsieve. Pores have diameter of 5 μm. The SEM micrograph on the right refers to a blank microsieve and the image on the left refers to a microsieve with a nanoporous membrane on top.

Figure 6. AFM images of a composite nanoporous membrane: detail of the microsieve with the nanoporous polymer membrane on top (a); corrected AFM image showing the coverage of the macropore by the polymer membrane (b); AFM profile corresponding to the horizontal line in Figure 6a (c); 3D AFM image showing the morphology of the nanoporous layer (d).

Figure 7. MB (squares) and BSA (triangles) diffusion through the composite membrane.